Phase behavior of the Stockmayer fluid via molecular dynamics simulation

Jörg Bartke and Reinhard Hentschke*
Fachbereich Mathematik und Naturwissenschaften, Bergische Universität, D-42097 Wuppertal, Germany
(Received 7 March 2007; revised manuscript received 3 May 2007; published 21 June 2007)

The gas-isotropic liquid-nematic liquid phase behavior of the Stockmayer fluid is studied using molecular dynamics simulation together with a mean field lattice model. We obtain coexistence curves of the Stockmayer fluid over a wide range of dipole strengths, temperatures, and densities, including the transition from the isotropic liquid to the ferroelectric liquid. In our simulations we do not observe the disappearance of the isotropic gas-isotropic liquid coexistence at high dipole strength contrary to earlier findings based on Monte Carlo techniques. Even though the formation of reversible dipole chains strongly affects the location of the critical point, it does not lead to its disappearance. These results are supported by a mean field lattice model which yields good qualitative, and in parts quantitative, agreement with our simulations. In addition, we also investigate the gas-isotropic liquid phase behavior for different polarizabilities.

DOI: 10.1103/PhysRevE.75.061503 PACS number(s): 64.70.Fx, 82.35.−x, 05.50.+q

I. INTRODUCTION

There are three simple models frequently studied in the context of dipolar liquids: the dipolar hard sphere (DHS) model, the dipolar soft sphere (DSS) model, and the Stockmayer (ST) model. Common to all three models is the description of long-range anisotropic interaction in terms of a (point) dipole- (point) dipole potential. They differ with respect to their short-range interaction. The DHS model employs hard core repulsion, whereas the ST potential employs the Lennard-Jones (LJ) potential. The intermittent DSS model adopts the soft repulsive core of the LJ potential. All three models exhibit a transition from an isotropic liquid to an orientationally ordered liquid, whereas a gas-liquid (GL) transition is established for the Stockmayer fluid only (e.g., Refs. [1–4]). Because attractive interaction is necessary for GL phase separation, the question is whether dipole-dipole interaction by itself may generate sufficient attraction to yield GL separation before another type of transition intervenes. The matter is complicated by the tendency of the dipole-dipole interaction to lead to the formation of reversible chains and, under certain conditions, rings [5]. This focusses the dipole-dipole interaction tangential to the chain. How much attractive interaction remains between different reversible aggregates, and whether this interaction is sufficient to yield GL phase separation in the DHS or DSS systems still is a matter of debate [3] (despite mounting evidence against the GL transition).

The ST model does exhibit GL phase separation readily for small dipole strengths, because of the LJ part of its potential. When the dipole strength is increased the GL phase separation previously was believed to disappear above a certain threshold. Expressed in terms of the reduced dipole moment μ, i.e., the dipole moment expressed in units of $\sqrt{4\pi\epsilon_o\epsilon\sigma^3}$ (ϵ_o: vacuum permittivity; ϵ and σ are the usual LJ parameters; in the following, $4\pi\epsilon_o=\epsilon=\sigma=1$), this threshold should be close to $\mu^2\approx 25$. This conclusion is based on work by van Leeuwen and Smit [6], which is quoted frequently in the subsequent literature (e.g., Refs. [4,7–12]). Van Leeuwen and Smit use the Gibbs-Ensemble Monte Carlo (MC) technique to study a variant of the ST potential, where the isotropic dispersion attraction is multiplied by a variable factor λ. However, their system may be mapped onto the ST system, which then leads to the above conclusion. A different conclusion was reached by Freed and co-workers based on a calculation using a mean field lattice model for reversibly associating polymers [13]. When they map the ST system onto their Flory-Huggins type lattice model they conclude that GL phase separation should occur for all dipole strengths. Recently we have extended this model and compared the critical point shift as a function of μ^2 to corresponding results derived from molecular dynamics (MD) computer simulations [14]. The model describes the μ^2 dependence of the GL critical point in good accord with our own simulation results as well as those of other groups. Particularly the μ dependence of the critical density can be explained in close analogy to the reduction of the critical density with increasing molecular weight in systems of linear polymers already discussed by Flory [15].

In this work we report the full GL phase coexistence curves, from which the above critical points were derived, obtained via MD simulations of the ST system. In particular we observe phase coexistence between an isotropic gas and an isotropic liquid for dipole strengths up to $\mu^2=36$, which is significantly above the limit proposed previously beyond which no GL transition should exist. To some extent we also include a discussion of the transition from the isotropic liquid to the ferroelectric liquid. The model of Ref. [14], which is applied here to describe the entire GL coexistence curve, is extended to include possible ferroelectric ordering. Finally, we also present GL coexistence curves of the polarizable Stockmayer fluid for point polarizabilities, α, in the range $0\leqslant\alpha\leqslant 0.08$ and dipole strengths $\mu^2=1.0, 2.0, 3.0$

The paper is structured as follows: Section II provides a detailed description of the MD methodology used to simulate the phase boundaries. In Sec. III we discuss the mean field lattice model and its mapping onto the ST system. In Sec. IV we present our MD results for the ST system including a

*Author to whom correspondence should be addressed. URL: http://constanze.materials.uni-wuppertal.de; hentschk@uni-wuppertal.de

comparison to the above mean field theory. This section also includes our results for the polarizable Stockmayer potential. Section V is the conclusion, where we discuss the implications of this work on the question of the existence of GL coexistence in DSS and DHS fluids.

II. MOLECULAR DYNAMICS METHOD

We carry out MD computer simulations of the (polarizable) Stockmayer fluid with the total potential energy

$$U = \frac{1}{2}\sum_{i,j=1}^{N} 4(r_{ij}^{-12} - r_{ij}^{-6}) - \frac{1}{2}\sum_{i=1}^{N} \vec{\mu}_i \cdot \vec{E}'(\vec{r}_i) \tag{1}$$

[16]. The first sum is over LJ pair potentials between the N particles. The second sum describes the interaction between point dipole moments $\vec{m}_i = \vec{\mu}_i + \vec{p}_i$, where $\vec{\mu}_i$ is a permanent dipole and $\vec{p}_i$ is an induced dipole, and the total field

$$\vec{E}'(\vec{r}_i) = \sum_{\substack{j \in V_{cut} \\ j \neq i}} \left[3\frac{(\vec{m}_j \cdot \vec{r}_{ij})\vec{r}_{ij}}{r_{ij}^5} - \frac{\vec{m}_j}{r_{ij}^3} \right] + \frac{2(\epsilon - 1)}{(2\epsilon + 1)r_{cut}^3} \sum_{j \in V_{cut}} \vec{m}_j. \tag{2}$$

Here $j \in V_{cut}$ means that we include all particles j inside a cutoff sphere with radius r_{cut} centered on particle i. We use the same cutoff for the LJ interactions, applying the usual continuum corrections beyond r_{cut}. The second sum describes all electrostatic interactions of i with particles beyond r_{cut} in terms of a homogeneous reaction field. Note that ϵ is the static dielectric constant of the fluid which *a priori* is unknown. The adequacy of the reaction field in comparison to infinite lattice sums was shown previously [18–20].

The translational motion of the particles as well as the rotation of the permanent dipoles $\vec{\mu}_i$ are integrated using the velocity Verlet algorithm. The equation of motion governing the dipole orientation follows via $\vec{N}_i = \vec{\mu}_i \times \vec{E}'(\vec{r}_i) = \mathcal{I}\ddot{\vec{\phi}}_i$. Here $\vec{N}_i$ is the torque acting on the fixed dipole moment $\vec{\mu}_i$, and $\mathcal{I}$ is the moment of inertia with respect to the momentary axis of rotation. The angle of rotation vector $\vec{\phi}_i$ can be replaced by $\vec{\mu}_i$ using $\dot{\vec{\phi}}_i \times \vec{\mu}_i = \dot{\vec{\mu}}_i$ and $\dot{\vec{\phi}}_i \cdot \vec{\mu}_i = 0$. The resulting equation of motion for $\vec{\mu}_i$ can be found in Sec. 8.2 of Ref. [21]. The rotational temperature is given by $(2\mu^2)^{-1}\langle \dot{\vec{\mu}}^2 \rangle = T$. (Notice that here we set the moments of inertia with respect to the major axes equal to one in LJ units.) Explicit expressions for the forces and torques were obtained by Vesely [22]. Temperature is controlled via the weak coupling method of Berendsen *et al.* [23]. The induced dipole moments are calculated at every MD step using the iteration scheme

$$\vec{p}_i^{\,k+1} = \alpha \vec{E}'(\vec{p}_i^{\,k}). \tag{3}$$

Here α denotes the isotropic polarizability of the particles. Note that only a small number of iteration steps, k, are sufficient to obtain satisfactory convergence. Note also that the value for ϵ is calculated as described in Ref. [17], i.e.,

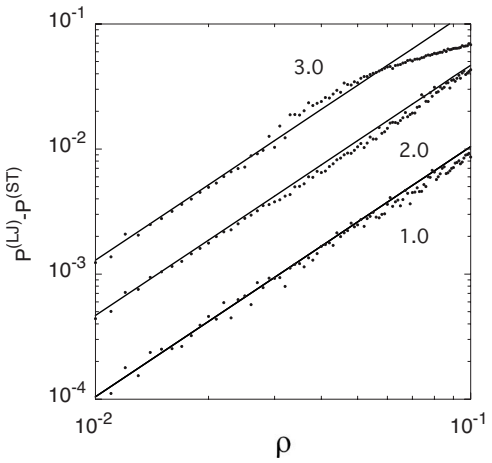

FIG. 1. LJ pressure, $P^{(LJ)}$, minus the pressure of the corresponding Stockmayer fluid, $P^{(ST)}$, vs particle number density, ρ, at $T = 1.2$. Symbols: simulation data; lines: second virial approximation, $\Delta P = T\rho^2[B_2^{(LJ)}(T) - B_2(T, \mu^2, 0)]$. Numbers are μ^2 values.

$$\frac{3}{4\pi\rho}\frac{(\epsilon - 1)(2\epsilon + 1)}{3\epsilon} = \frac{\langle \vec{M}_{sphere} \cdot \vec{M} \rangle_{\vec{E}=0}}{TN_{sphere}} + \frac{3}{4\pi\rho}\frac{(\epsilon_\infty - 1)(2\epsilon_\infty + 1)}{3\epsilon_\infty}. \tag{4}$$

Here ρ is the particle number density, $\vec{M}_{sphere}$ is the total dipole moment of the cutoff sphere containing N_{sphere} dipoles, whereas $\vec{M}$ is the dipole moment of the entire simulation box. The index relation, $\vec{E} = 0$, refers to an external field. ϵ_∞ is related to α via the Clausius-Mossotti relation. It is the cumulative average of ϵ thus obtained which is used to calculate $\vec{E}'$.

A number of comparisons between MD and analytic results are shown in Figs. 1–3. Figure 1 shows the difference $P^{(LJ)} - P^{(ST)}$ vs particle number density, ρ, at low densities for $T = 1.2$ and $\mu^2 = 1, 2, 3$. Here $P^{(ST)}$ is the pressure of the Stockmayer fluid and $P^{(LJ)}$ is the pressure of the same system, but with $\mu^2 = 0$. The solid lines are obtained based on a second virial approximation as discussed in the Appendix. We do include this figure primarily as a check of the accuracy of our MD program because dipolar systems are rather complex and programming errors are not unlikely. In Fig. 2, a similar comparison is shown for $T = 1.2$ and $\mu^2 = 3$, but with nonzero point polarizability, α. In the following, however, we set $\alpha = 0$ unless stated otherwise.

GL phase coexistence curves are obtained primarily via Maxwell construction. We carry out a large number of *NVT* simulations along an isotherm, an example is shown in Fig. 4, which allows us to employ the Maxwell construction to obtain the coexisting densities for the pure gas and the pure liquid, respectively. Repeating this procedure for a series of temperatures yields the GL coexistence curve, which we analyze using the well known scaling relations, i.e., $\rho_L - \rho_G \approx A_o|t|^\beta + A_1|t|^{\beta+\Delta}$, $(\rho_L + \rho_G)/2 \approx \rho_c + D_o|t|^{1-\alpha} + D_1|t|$, and $P - P_c \approx P_o|t| + P_1|t|^{2-\alpha} + P_2|t|^2$ [$t = (T - T_c)/T_c$] [24], in conjunction with the Ising values of the critical exponents α

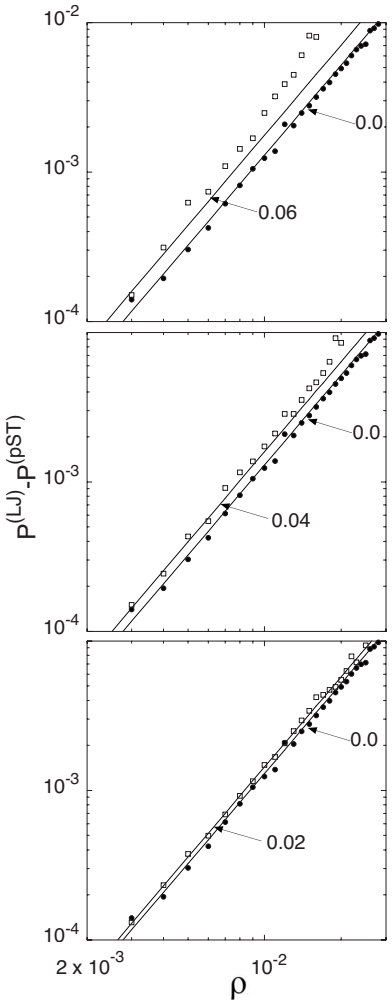

FIG. 2. LJ pressure, $P^{(LJ)}$, minus pressure of the corresponding polarizable Stockmayer fluid, $P^{(pST)}$, vs particle number density, ρ, for $\mu^2=3.0$ and $T=1.2$. Symbols: simulation data; lines: second virial approximation, $\Delta P=T\rho^2[B_2^{(LJ)}(T)-B_2(T,\mu^2,\alpha)]$. Numbers with arrows indicate the α values.

≈ 0.110 (not to be confused with the polarizability), $\beta \approx 0.326$, and $\Delta \approx 0.5$ [25] to extract the critical point parameters.

As a check of the Maxwell construction method we compare in Fig. 5 selected results to corresponding results obtained via thermodynamic integration using Kofke's method [26,27]. In addition we vary the system size, N, cutoff, r_{cut}, and the temperature increment, ΔT (in the case of thermodynamic integration). The coexistence curves thus obtained for selected fixed dipole strengths are in close accord.

III. LATTICE MODEL

In Ref. [14] we have developed a theoretical description of the Stockmayer fluid based on a Flory-Huggins–like lattice free energy, i.e., occupied cells (representing single dipoles) on a cubic lattice may form polymer chains of variable length via side-by-side reversible association. Here we summarize the essential formulas for clarity. The lattice free

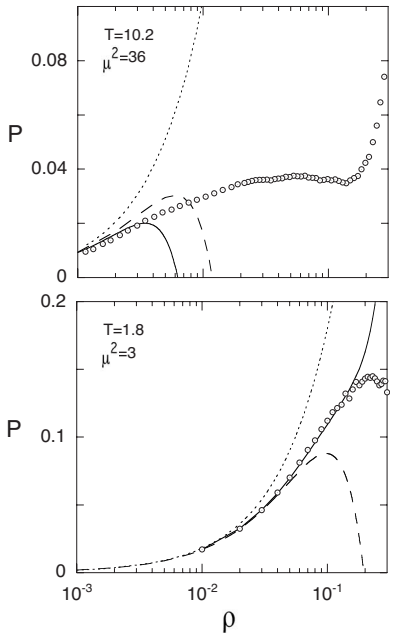

FIG. 3. Pressure, P, vs number density, ρ. The lines are analytic results corresponding to the ideal gas equation of state (dotted line) and virial approximations including the second (dashed line) and third (solid line) virial coefficient, respectively. Top: $T=10.2$, $\mu^2=36$; bottom: $T=1.8$, $\mu^2=3$.

energy expressed in terms of the overall volume fraction of Stockmayer particles, ϕ, is given by

$$\frac{b_o F_{config}}{TV} = \phi \ln \phi + (1-\phi)\ln[1-\phi] + \frac{1}{2}q\varepsilon\phi^2 + \left(1 - \frac{1}{n} - 2\ln[n]\right)\phi, \tag{5}$$

where

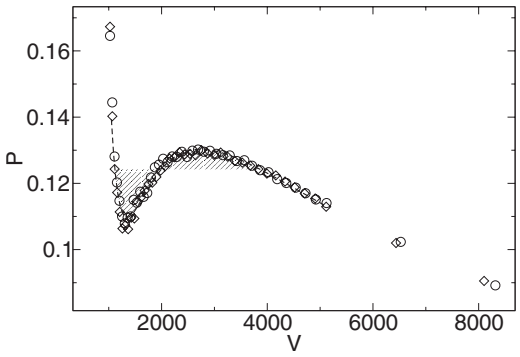

FIG. 4. Illustration of the Maxwell construction method. The symbols are the results of *NVT*-MD simulations. Open circles: results obtained during compression; open diamonds: results obtained during subsequent expansion. The dashed line represents a fit using a simple approximate equation of state. The shading highlights the equal areas.

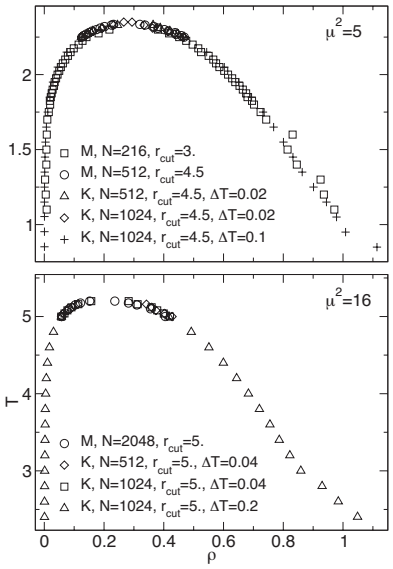

FIG. 5. Binodal lines in the T-ρ plane for $\mu^2=5$ (top) and $\mu^2=16$ (bottom). Comparison of methods (M: Maxwell construction; K: Kofke integration).

$$n = \frac{1}{2} + \frac{1}{2}\sqrt{1 + 20\phi e^{-\varepsilon_i}} \tag{6}$$

is the average length of the reversible dipole chains. The interchain and intrachain particle-particle interaction parameters $q\varepsilon$ and ε_i are defined and computed as in Ref. [14], i.e.,

$$\varepsilon q = -\frac{4T_{c,LJ}}{T} - \frac{16\pi}{9b_o R^3}\frac{\mu^4}{T^2}, \tag{7}$$

where $T_{c,LJ}$ is the critical temperature of the Lennard-Jones system, b_o is the particle volume, $R=4.1$ is a parameter, and ε_i is a free energy gain per dipole-dipole contact along a chain [cf. Eq. (25) in the above reference]. Notice that the volume fraction is related to the number density, ρ, via $\phi = b_o\rho$. From the equation of state,

$$\frac{b_o P_{config}}{T} = -\left(1 - \frac{1}{n}\right)\phi + \frac{1}{2}q\varepsilon\phi^2 - \ln[1-\phi], \tag{8}$$

in conjunction with the chemical potential, $\mu = F/N + b_o P/\phi$, we compute the GL coexistence curve via simultaneous solution of $P(T,\phi_g) = P(T,\phi_l)$ and $\mu(T,\phi_g) = \mu(T,\phi_l)$, where ϕ_g and ϕ_l are the coexisting volume fractions of gas (g) and liquid (l).

This model does not yet include ferroelectric order. A mean field description of ferroelectric order is based on the orientation partition function

$$Q_{orient} = \frac{N!}{\Pi_\nu N_\nu!(4\pi/\Delta\Omega)^N}\exp\left(\frac{1}{2T}\sum_{i=1}^{N}\vec{E}_{loc}^{(D)}\cdot\vec{\mu}_i\right). \tag{9}$$

Here N_ν is the number of dipoles oriented along the solid angle Ω_ν, $(4\pi/\Delta\Omega)^N$ is the total number of orientational states, and $\vec{E}_{loc}^{(D)}$ is given by

$$\vec{E}_{loc}^{(D)} = \frac{4\pi\rho}{3}\frac{\epsilon+2}{\epsilon-1}\langle\vec{\mu}\rangle. \tag{10}$$

This expression due to Debye [28] is an approximation of the local electric field experienced by a point dipole in the center of a spherical cavity inside a dielectric medium with a static dielectric constant ϵ. The attending orientation free energy is

$$\frac{b_o F_{orient}}{VT} = \phi\left(\left[\frac{3}{2} - \frac{2\pi\rho\mu^2}{3T}\right]s^2 + \frac{9}{20}s^4 + \frac{99}{350}s^6 + \frac{1539}{7000}s^8\cdots\right), \tag{11}$$

where μs is the average dipole moment along the director. In addition $\frac{\epsilon+2}{\epsilon-1}$ is set equal to unity. When the coefficient of the leading term changes sign an orientationally ordered phase becomes stable compared to the isotropic fluid or vice versa. The equilibrium value of s, i.e., $s^{(o)}$, is determined by $\partial\frac{b_o F_{orient}}{VT}/\partial s|_{T,\phi}=0$. Thus the combined free energy is $F = F_{config} + F_{orient}(s^{(o)})$. The combined pressure is $P = P_{config} + P_{orient}(s^{(o)})$, where

$$\frac{b_o P_{config}}{T} = -\frac{2\pi\phi^2\mu^2}{3T}(s^{(o)})^2. \tag{12}$$

With the exception of possible chain formation this model has been used before by Zhang and Widom [29] to investigate the global phase diagram of dipolar fluids (Zhang and Widom use the van der Waals free energy to model F_{config}).

The condition $3/2 - 2\pi\rho\mu^2/(3T_{c,f}) = 0$ yields an isotropic-ferroelectric transition temperature, $T_{c,f} = \frac{4\pi}{9}\rho\mu^2$, which is considerably too high. In fact, the absence of experimental evidence for a ferroelectric transition in molecular liquids motivated an alternative to Debye's approach due to Onsager, also based on continuum electrostatics of a single dipole within a spherical cavity, which does not yield a transition at all (for details see Ref. [17]). However, there are numerous computer simulation studies on model systems such as dipolar hard and soft spheres or the Stockmayer fluid, which do find a transition from an isotropic liquid to an orientationally ordered liquid. In addition there are also experiments lending support to the existence of such a transition in reality (cf. again Ref. [17] for a detailed discussion; a recent large scale simulation study addressing this issue is described in Ref. [30]). Here we account for these results by scaling the Debye transition temperature, $T_{c,f}^{(D)}$ via $T_{c,f} = \kappa T_{c,f}^{(D)}$, where $\kappa \approx 0.1361$ is chosen to reproduce the transition temperature $T_{c,f}^{(ST)}$ obtained on the basis of previous simulation work [17].

IV. COMPARISON BETWEEN MOLECULAR DYNAMICS SIMULATION AND LATTICE MODEL

Figure 6 compiles coexistence curves for dipole strengths in the range from $\mu^2=0$ to $\mu^2=36$ obtained via Maxwell construction (numerical values for critical temperatures and densities are listed in Table I). We note that the critical temperature obtained for the LJ system is slightly higher than most values found in the literature (between 1.31 to 1.32).

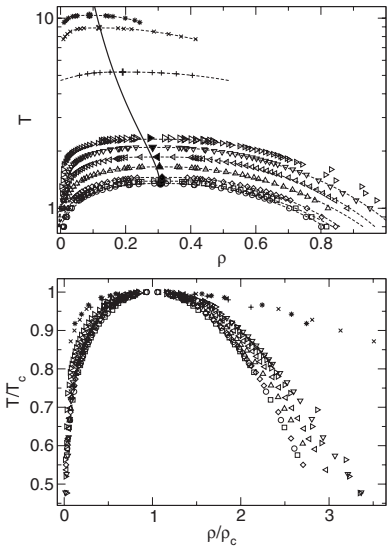

FIG. 6. Top: GL coexistence curves in the temperature-density plane obtained in this work. The different symbols are MD data obtained for $\mu^2=0$ (circles), 0.5 (squares), 1.0 (diamonds), 2.0 (up triangles), 3.0 (left triangles), 4.0 (down triangles), 5.0 (right triangles), 16 (plusses), 30 (crosses), and 36 (stars). Fat symbols indicate the position of the critical point. The dashed lines are fits obtained via the scaling relations provided in the text. The solid line shows the shift of the critical point as obtained by the lattice theory. Bottom: Same as above in reduced units (T_c: GL critical temperature; ρ_c: GL critical number density).

Possibly the equal area construction based on a simple equation of state, such as the van der Waals equation or modifications of the van der Waals equation, overemphasizes the occurrence of the pressure loop. Nevertheless, this effect is small compared to the dependence of the GL critical temperature on μ^2 in the range studied.

Notice also that for $\mu^2=16$ the Kofke data shown in Fig. 5 cover a larger density interval in comparison to the Maxwell construction data shown here. While our simulations are in close accord with previous works for dipole strengths $\mu^2<25$ [6,7,31–34], we do find phase coexistence also for the larger dipole strengths. This disagrees with the Gibbs-Ensemble MC work by van Leeuwen and Smit [6], which is responsible for the widely accepted belief that the Stockmayer system should not exhibit a GL critical point above $\mu^2\approx 25$.

Even though van Leeuwen and Smit (vLS) study a modified version of the Stockmayer potential, in which the isotropic dispersion attraction term is multiplied by a variable factor λ, their system can be mapped onto the ordinary Stockmayer system (cf. [7] or [14]) via $T_{ST}=\lambda^{-2}T_{vLS}$, $\rho_{ST}=\lambda^{-1/2}\rho_{vLS}$, and $\mu_{ST}=\lambda^{-3/4}\mu_{vLS}$. The index ST indicates the normal Stockmayer potential, whereas the index vLS refers to the modified potential in Ref. [6]. In particular the limit $\lambda\to 0$, the soft-sphere potential, corresponds to the large dipole moment limit in the ST system (we return to this point below).

Van Leeuwen and Smit attribute the observed disappearance of the critical point to the formation of reversible dipole chains. A different conclusion was reached by Freed and coworkers who study the interplay between chain formation and GL phase separation using a mean field (Flory-Huggins) lattice model [13]. According to them the GL critical point should exist for all dipole strength. Using an extended version of their model we were able to describe the shift of the critical point as a function of dipole strength in good accord with the existing simulation data (including the results in this work) (cf. Fig. 3 in Ref. [14]). One result obtained by this model is the solid line in Fig. 6 (top panel), which is the path of the critical point in the T-ρ plane parametrized by the dipole moment. In particular, the shift of the critical density is directly related to the formation of reversible chains whose mean length increases with increasing μ. In Ref. [14] we discuss the strong similarity of this behavior with the critical point shift in systems of ordinary n alkanes, where $\rho_c\sim n^{-1/2}$ for large n (cf. [15]). It is this similarity which also makes the disappearance of the GL critical point in the ST system due to chain formation highly suspicious. As the alignment of the dipoles tangential to the chain strongly diminishes the dipole-dipole interaction between chains, the remaining LJ interaction makes the chains very much alkanelike.

On the other hand the dipole-dipole interaction may give rise to long-range orientational order, and the attending transition from the isotropic fluid to an anisotropic liquid may interfere with the isotropic gas-to-isotropic liquid transition. Zhang and Widom [29] have studied the interplay between isotropic van der Waals type interaction and anisotropic di-

TABLE I. GL critical parameters for the ST system and the polarizable ST system.

μ^2	α	T_c	ρ_c	P_c
0	0.00	1.35	0.307	0.147
0.5	0.00	1.39	0.309	0.156
1	0.00	1.45	0.3123	0.158
2	0.00	1.65	0.304	0.168
3	0.00	1.86	0.297	0.170
4	0.00	2.09	0.283	0.170
5	0.00	2.34	0.275	0.159
16	0.00	5.20	0.191	0.121
30	0.00	8.89	0.118	0.0668
36	0.00	10.35	0.089	0.0439
1	0.02	1.48	0.297	0.160
1	0.04	1.50	0.308	0.160
1	0.06	1.53	0.307	0.162
1	0.08	1.58	0.308	0.175
2	0.02	1.69	0.307	0.164
2	0.04	1.76	0.316	0.174
2	0.06	1.85	0.310	0.189
2	0.08	1.95	0.321	0.203
3	0.02	1.95	0.297	0.175
3	0.04	2.07	0.303	0.186
3	0.06	2.22	0.304	0.210
3	0.08	2.43	0.322	0.240

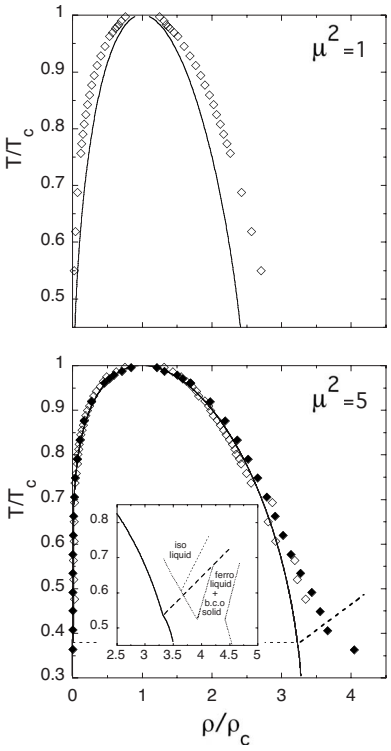

FIG. 7. Comparison between simulation (symbols) and lattice theory (lines) for the indicated dipole strength. Open symbols: Maxwell construction; solid symbols: Kofke integration. The thick-dashed line indicates the transition from the isotropic to the ferroelectric liquid. The inset shows a comparison between the lattice theory for $\mu^2=6.25$ and the corresponding section of the phase diagram obtained via simulation in Ref. [37] (dotted and short dashed lines).

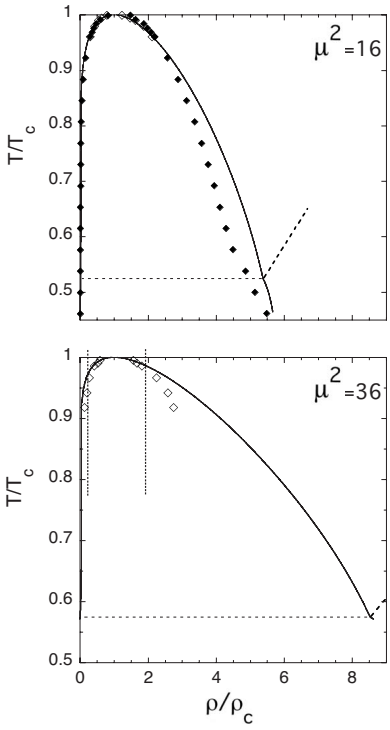

FIG. 8. Comparison between simulation (symbols) and lattice theory (lines) for the indicated dipole strength. Symbols and lines correspond to the previous figure. The vertical dotted lines in the bottom panel are explained in the text.

polar interaction using a simple mean field model. The difference to the model used in this work is the neglect of chain formation, i.e., F_{config} is modeled in terms of the van der Waals form of the free energy. The authors obtain a sequence of phase diagrams which indicate a vanishing of the GL critical point due to the instability of the isotropic liquid in comparison to the anisotropic liquid. The parameter which drives this behavior is the reduction of the GL critical temperature. Similar results were obtained via density functional theory by Groh and Dietrich [35,36]

With the same idea in mind we compute the phase diagram of the ST system including possible ferroelectric ordering using our mean field model. The results are compiled in Figs. 7 and 8. Obviously the transition to the ferroelectric state occurs at rather low temperatures. Of the three typical phase diagrams discussed by Zhang and Widom in their Fig. 2, only the topmost diagram appears to be realized in the ST system. We should note that our mean field theory contains two adjustable parameters. The parameter R introduced in Eq. (12) in Ref. [14] is fixed by the rise of the GL critical temperature shown in Fig. 3 of this reference. Here we use the same value. The second parameter is κ. The latter reduces the Debye transition temperature to the ferroelectric state, which is too high, to the value obtained in Ref. [17]. We note that the nematic order parameter computed during the simulations with $\mu^2=5$ and $\mu^2=16$ increases significantly above zero for those liquid densities at low temperatures, i.e., $T/T_c<0.4$ for $\mu^2=5$ and $T/T_c<0.55$ for $\mu^2=16$, which appear to deviate from the extrapolated coexistence curve based on the densities at higher T/T_c. This is illustrated by the two simulation snapshots shown in Fig. 9. The lower panel depicting a system configuration at $T/T_c\approx0.36$ exhibits visible orientational order. We also note that the other phase diagrams obtained by Zhang and Widom in their Fig. 3 do follow from our mean field model if the parameter κ is increased. However, this is not appropriate for the ST system. Notice that the inset in the lower panel of Fig. 7 shows a partial phase diagram obtained for $\mu^2=6.25$ and a slightly increased value of κ ($\kappa=0.186$) in comparison to a partial phase diagram obtained via simulation by Gao and Zeng [37]. These authors primarily have studied the additional transition to the solid state not studied in this work. In summary, it is unlikely that the transition to ferroelectric ordering will cause the GL critical point to disappear. Certainly this is not the case in the range of dipole strengths considered here. Note also that even though, according to the Debye theory, $T_{c,f}$, the ferroelectric transition temperature, increases proportional to μ^2 at fixed ρ, the same dependence, i.e., $T_c \propto \mu^2$ for large μ, is found for the GL critical temperature. In addition the GL critical point "escapes" to lower densities.

Ferroelectric ordering, as considered thus far, is induced by the particle's dipole moments. Another cause for possible orientational order, at least theoretically, is shape induced interaction between reversible chains akin to the isotropic-to-nematic phase transition studied originally by Onsager for rigid monodisperse rods or rodlike polyelectrolytes [38]. The

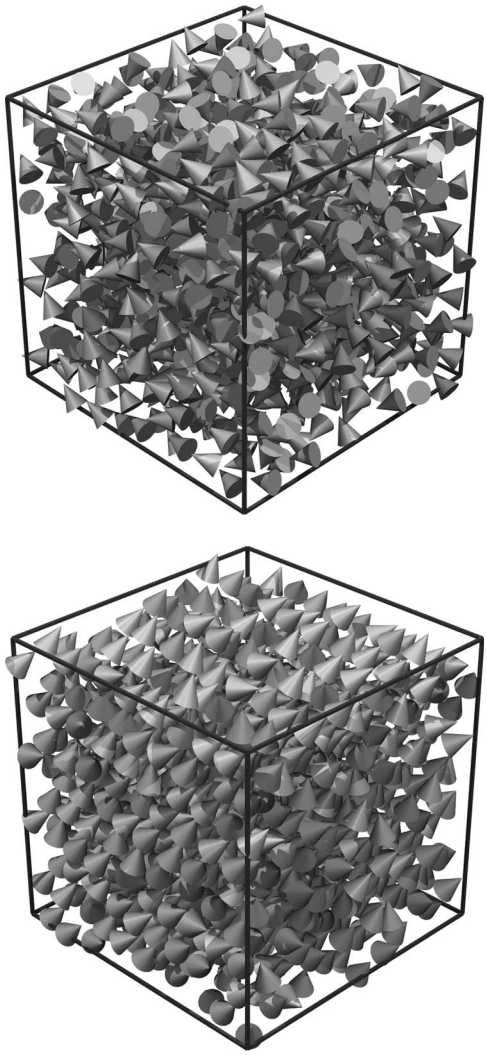

FIG. 9. Simulation snapshots of the $\mu^2=5$ system. Top: $T/T_c \approx 0.49$; bottom: $T/T_c \approx 0.36$. Every ST particle is represented by a cone indicating the instantaneous orientation of the dipole moment.

transition to the nematic state occurs for volume fractions proportional to d/L, where d is an effective rod diameter and L is the rod length. For large L the transition therefore occurs at small densities. Onsager's approach can be extended to semiflexible polymers (cf. [39,40]) and to rodlike micelles (cf. [41]). In these theories an orientationally ordered phase occurs for volume fractions proportional to d/P_L, where P_L is the persistence length, a measure for the chain stiffness. Notice that P_L depends on temperature. The fact that such a transition is not observed in the ST system may be understood in terms of the small persistence length, but for other models of equilibrium polymers this may be relevant [42,43].

Figure 10 shows the average chain length, n, along the GL coexistence curve obtained for $\mu^2=16$. The symbols are simulation results, whereas the solid line is the theoretical result. First we note that two Stockmayer particles are considered to be neighbors along the same chain if their distance is less than r_n. Because this is a rather simple criterion it produces somewhat different results for $r_n=1.0$ and $r_n=1.2$. Nevertheless, we note that there is qualitative agreement between the lattice theory and the simulation similar to the case of the average chain length at criticality shown in Fig. 5 of Ref. [14].

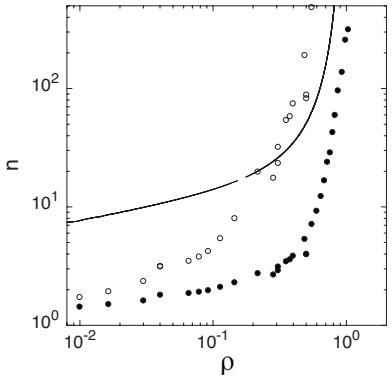

FIG. 10. Mean aggregation number, n, vs particle number density, ρ, along the GL coexistence curve for $\mu^2=16$. Symbols: simulation result obtained with $r_n=1.0$ (solid circles) and $r_n=1.2$ (open circles); solid line: lattice theory. Note that the gap in this curve indicates the critical point.

In Fig. 11 we compare the temperature dependence of the isochoric heat capacity per particle, C_V (omitting the contributions from the kinetic degrees of freedom), obtained via canonical MC simulation in Ref. [12] for $\mu^2=36$, to the lattice theory. Again there is qualitative agreement. It is important to note that our theoretical treatment neglects the revers-

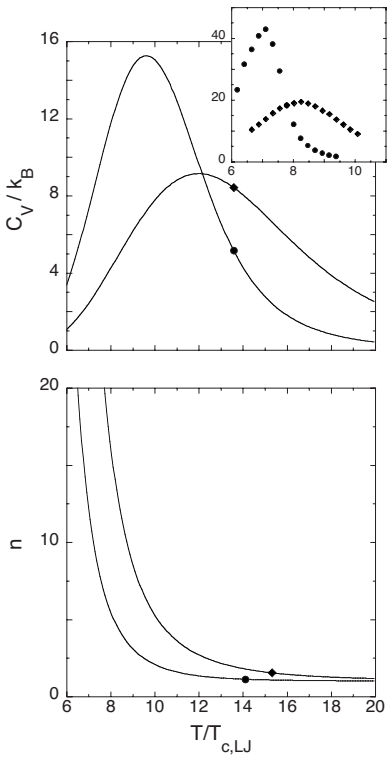

FIG. 11. Top: Heat capacity, C_V, vs reduced temperature, $T/T_{c,LJ}$. Diamond: $\rho/\rho_{c,LJ}=0.0637$; circle: $\rho/\rho_{c,LJ}=0.00637$. $T_{c,LJ}$ and $\rho_{c,LJ}$ are critical quantities of the LJ system. Inset: Corresponding heat capacity via canonical Monte Carlo simulation taken from Ref. [12] (Fig. 4). Bottom: Corresponding average chain length, n.

ible formation of loops. In Ref. [12] it is shown, however, that there may be a large fraction of loops at the thermodynamic conditions considered here. Notice in this context that the theoretical C_V in Fig. 11 is almost exclusively determined by the last term in Eq. (5) [b_o and therefore ϕ is slightly dependent on temperature via Eq. (26) in Ref. [14]], i.e., C_V is determined by the temperature dependence of the average chain length, n. The latter is shown in the bottom panel. The strongest curvature of n as a function of T, i.e., the onset of aggregation, corresponds to the maximum of the heat capacity. As explained in Ref. [14] the no-aggregation limit of the lattice theory is not $n=1$ but $n\approx 2$. We also note that the authors of Ref. [12] apparently do not notice phase coexistence even though their isochors cross from the one phase into the coexistence region found in our simulations (as indicated by the vertical dotted lines in the bottom panel of Fig. 8).

We briefly want to return to the issue of relative stability of chains and loops mentioned above. The probability for an ideal wormlike chain containing N dipoles to form a loop is $p_{loop}=(4\pi)^{-1}[3/(2\pi N)]^{3/2}$ [44]. Notice that a random path maps out a sphere of radius $\sim N^{1/2}$ and volume $\sim N^{3/2}$. The factor $(4\pi)^{-1}$ accounts for the smoothness of the chain at the junction point. The remaining factor results from the normalization of the random path's probability distribution. Using $p_{chain}=1-p_{loop}$ we obtain the entropy loss due to ring closure $\Delta S=S_{loop}-S_{chain}=\ln(p_{loop}/p_{chain})$. The corresponding change of the free energy is $\Delta F=T\epsilon_i-T\ln(p_{loop}/p_{chain})$. Here $T\epsilon_i$ is the contribution of the contact interaction to the free energy [cf. Eq. (25) in Ref. [14]]. The condition $\Delta F=0$ thus defines the crossover length, $N_x\sim\exp(-2\epsilon_i/3)$, for sufficiently large N. This means that for $N>N_x$ the chain is more stable than the loop, whereas for $N<N_x$ the loop is more stable than the chain. On the other hand, according to Eq. (6), the lattice model yields a mean chain length $n\sim\phi^{1/2}\exp(-\epsilon_i/2)$. If we are interested in the relative stability of chains vs loops close to GL criticality we can make use of $\phi_c\sim n_c^{-1/2}$, where the index c indicates the critical values, which follows from Eq. (6) in Ref. [14] for large n_c (corresponding to large μ^2). Therefore we find $n_c\sim N_x^{3/5}$, which means close to the GL critical point, for sufficiently large μ^2 and therefore large n_c (cf. Fig. 5 in Ref. [14]), loops are more stable than chains. We return to this point in the conclusion section.

Finally, we return to the polarizable ST model. Figure 12 compiles GL coexistence curves we obtain at fixed dipole moment ($\mu^2=1$) for different values of the point polarizability, α, using again the Maxwell construction method. The critical parameters are listed in Table I together with additional results for $\mu^2=2$ and $\mu^2=3$. Figure 13 shows the α dependence of the critical temperature for $\mu^2=1$, 2, and 3. Here the ratio $T_c/T_{c,LJ}$ is estimated using its relation to the Boyle temperature, T_{Boyle}, defined via $B_2(T_{Boyle},\mu,\alpha)=0$, i.e., $T_c/T_{c,LJ}=T_{Boyle}/T_{Boyle,LJ}$. The index LJ always refers to the same quantity in the LJ system. We obtain this estimate by computing the critical temperature from Eq. (8) for $n=1$, i.e., $T_c=-q\varepsilon_o/4$, where the temperature dependence of ε in Eq. (8) is described via $\varepsilon=\varepsilon_o/T$. If in addition we expand the pressure to second order in ϕ we obtain the second virial coefficient $B_2(T)$. Solving $B_2(T)=0$ for T yields $T_{Boyle}=4T_c$.

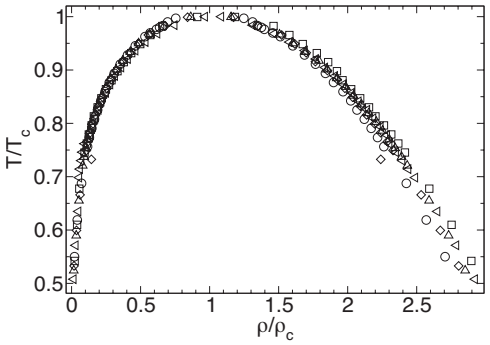

FIG. 12. GL coexistence curve in critical units for $\mu^2=1$. Circles: $\alpha=0$; squares: $\alpha=0.02$; diamonds: $\alpha=0.04$; up triangles: $\alpha=0.06$; left triangles: $\alpha=0.08$.

Notice that this estimate of T_c in terms of T_{Boyle} coincides or is close to the corresponding result obtained from other simple equations of state such as the Dieterici or van der Waals equations of state. Because the dipole strength is low, we can neglect chain formation. The resulting estimate of T_c via T_{Boyle} is in qualitative agreement with the simulation data.

V. CONCLUSION

In this work we mainly present the results of MD simulations for GL coexistence in the Stockmayer system. While corresponding results have been reported before for smaller dipole strengths [6,7,31–34], here we study large dipole strengths for which it was believed previously that no GL coexistence should exist. However, we do find coexistence of the isotropic gas and the isotropic liquid for all dipole strengths studied, i.e., $0\leqslant\mu^2\leqslant 36$. Our findings are supported by a mean field model based on the Flory-Huggins description for polymer solutions.

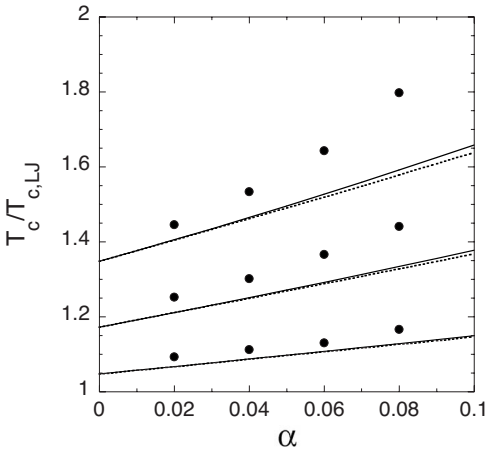

FIG. 13. GL critical temperature, T_c, in units of the LJ GL critical temperature, $T_{c,LJ}$, vs polarizability, α. From bottom to top: $\mu^2=1,2,3$. The symbols are simulation data taken from Table I. Solid lines show the theoretical result including the second order in α; dotted lines show the theoretical result including the first order in α.

At this point we want to discuss the implications of the present work on the existence of GL phase separation in the DSS system. As mentioned above, van Leeuwen and Smit [6] have used the following potential,

$$\frac{U_{vLS}(r_{vLS},\mu_{vLS})}{T_{vLS}} = \frac{4}{T_{vLS}}\left(\frac{1}{r_{vLS}^{12}} - \lambda\frac{1}{r_{vLS}^{6}}\right) - \frac{\mu_{vLS}^2}{T_{vLS}r_{vLS}^3}f, \tag{13}$$

where f simply is a function of the relative orientation of two interacting dipoles, instead of the Stockmayer potential,

$$\frac{U_{ST}(r_{ST},\mu_{ST})}{T_{ST}} = \frac{4}{T_{ST}}\left(\frac{1}{r_{ST}^{12}} - \frac{1}{r_{ST}^{6}}\right) - \frac{\mu_{ST}^2}{T_{ST}r_{ST}^3}f, \tag{14}$$

in order to study the effect of variable isotropic attraction. However, as already pointed out by others (cf. sec. II in Ref. [7]), the two formulas for U/T are related via $T_{ST}=\lambda^{-2}T_{vLS}$, $\rho_{ST}=\lambda^{-1/2}\rho_{vLS}$, and $\mu_{ST}=\lambda^{-3/4}\mu_{vLS}$. If we consider the vLS system at fixed dipole moment, i.e., $\mu_{vLS}=const$, then $\lambda\to 0$ implies $\mu_{ST}\to\infty$. According to Ref. [14] as well as this work we have $T_{c,ST}\sim\mu_{ST}^2$ for large μ_{ST}, and therefore $T_{c,vLS}\sim\lambda^2\mu_{ST}^2=\lambda^{1/2}\mu_{vLS}\to 0$ for $\lambda\to 0$. For the critical density we have $\rho_{c,vLS}=\lambda^{1/2}\rho_{c,ST}$. Again according to Ref. [14] as well as this work $\rho_{c,ST}$ decreases monotonically with increasing μ_{ST}. This yields $\rho_{c,vLS}\to 0$ for $\lambda\to 0$. Because the $\lambda\to 0$ limit corresponds to the DSS fluid, the latter should not exhibit GL coexistence. Due to the strong similarity between the DSS and the DHS system, we expect the same conclusion to hold for DHS.

Nevertheless, there may be other types of phases and phase transitions, which are not included at present. Loops, as we have discussed above, may become dominant compared to chains at high dipole strength, when the GL critical point has shifted to low densities. However, there is no compelling reason to expect that loops and chains should phase separate under these conditions. A different suggestion is due to Tlusty and Safran [45]. They argue that reversible chains may form reversible networks. The chain ends may participate in reversible, threefold coordinated crosslinks or may be free. The authors construct a free energy based solely on the network defects, i.e., the free ends and the crosslinks. They find that phase separation into a free end-rich and a free end-poor phase can occur. The whole idea is developed on the basis of the DHS model. The model is a much simplified theory for a (reversible) polymer network. Other types of defects may be present and important, e.g., physical crosslinks. In particular, as the authors remark themselves, a crucial prerequisite is the observation of dipolar networks. However, the simulations presented in this work as well as a number of exploratory simulations for $\mu^2=100$ at $T=26.5$, extrapolating the linear dependence of the critical temperature in Fig. 3 of Ref. [14], and various low densities, $\rho=0.001$, 0.01, 0.05 do not reveal network formation in the Stockmayer system. (We note that we do find a van der Waals loop for $\mu^2=100$ at $T=22$ and $T=24$. The full calculation necessary to locate the critical point, however, is too time consuming at present.)

APPENDIX: SECOND VIRIAL COEFFICIENT FOR THE STOCKMAYER POTENTIAL INCLUDING POLARIZATION

The (maximum term) classical partition function for a system of N Stockmayer dipoles is given by

$$Q = \frac{1}{N_1!N_2!\ldots(4\pi/\Delta\Omega)^N(2\pi\hbar)^{5N}} \times \int d\{\vec{p},\vec{r}\}d\{\phi,\theta,p_\phi,p_\theta\}e^{-\beta\mathcal{H}}.$$

Here N_ν is the number of indistinguishabel dipoles pointing into a solid angle element $\Delta\Omega_\nu=\Delta\Omega$ $(N=\Sigma_\nu N_\nu)$, and $(4\pi/\Delta\Omega)^N$ is the total number of orientational states [46]. The integral is over all translational coordinates and momenta as well as over all Euler angles, specifying the dipole orientations, and their conjugate momenta. The Hamiltonian is given by

$$\mathcal{H} = \sum_{j=1}^{3N}\left(\frac{1}{2}\mathcal{I}_j\omega_j^2 + \frac{p_j^2}{2m}\right) + U(\{r\},\{\phi\},\{\theta\}), \tag{A1}$$

where $\mathcal{I}_1=\mathcal{I}_2=\mathcal{I}$ and $\mathcal{I}_3=0$. Notice that the potential energy U does not depend on the Euler angle ψ, because rotation with respect to the dipole's axis has no effect. Thus we have used $\psi=0$. We now proceed in standard fashion by transforming the integrations over the momenta conjugate to the Euler angles to the angular velocities ω_j with respect to the major axes (e.g., [47]). The result is

$$-\ln Q = -N\ln\left[\frac{2\mathcal{I}}{\beta\hbar^2}\right] + N\ln(4\pi\Lambda_T^3\rho/\Delta\Omega) + \sum_\nu\left(N_\nu\ln\frac{N_\nu}{N} - N_\nu\right) - \ln\int\frac{d\{\vec{r}\}}{V^N}d\{\phi,\theta\sin\theta\}e^{-\beta U}. \tag{A2}$$

Here we have made use of the Stirling approximation for the N_ν. The quantity Λ_T is the thermal wavelength, and ρ is the dipole number density. A second order virial expansion yields the free energy

$$\frac{\beta F}{N} = -\ln\left[\frac{8\pi\mathcal{I}}{\beta\hbar^2}\right] + \ln(\Lambda_T^3\rho) - 1 + \int\frac{d\Omega}{4\pi}f(\Omega)\ln f(\Omega) + \rho B_2(T) + \mathcal{O}(\rho^2), \tag{A3}$$

where the second virial coefficient is given by

$$B_2(T) = -\frac{1}{2}\int\frac{d\Omega d\Omega'}{(4\pi)^2}f(\Omega)f(\Omega')\int d^3r(e^{-\beta u(\vec{r},\Omega,\Omega')} - 1). \tag{A4}$$

Notice that Ω denotes the dependence on ϕ and θ $(d\Omega=d\phi d\theta\sin\theta)$, and $\Delta\Omega f(\Omega_\nu)=4\pi N_\nu/N$ is the dipole orientation distribution function $(\int d\Omega f/4\pi=1)$.

In the present case the pair interaction potential $u(\vec{r},\Omega,\Omega')$ is

TABLE II. Additional terms in the expression for $B_2(T,\mu^2,\alpha)$ in Eq. (A11).

$\mathcal{O}(\alpha^0)$	$\mathcal{O}(\alpha^1)$	$\mathcal{O}(\alpha^2)$
$\frac{x^2}{3}h_1$	$2xh_1$	$\frac{21x^2}{5}h_2$
$\frac{x^4}{25}h_2$	$\frac{4x^3}{5}h_2$	$\frac{836x^4}{525}h_3$
$\frac{29x^6}{11025}h_3$	$\frac{58x^5}{525}h_3$	$\frac{269x^6}{1225}h_4$
$\frac{11x^8}{99225}h_4$	$\frac{88x^7}{11025}h_4$	$\frac{5794x^8}{363825}h_5$
$\frac{13x^{10}}{4002075}h_5$	$\frac{26x^9}{72765}h_5$	$\frac{10139x^{10}}{14189175}h_6$
$\frac{17x^{12}}{243486243}h_6$	$\frac{68x^{11}}{6243237}h_6$	$\frac{73732x^{12}}{3381753375}h_7$
$\frac{523x^{14}}{456536705625}h_7$	$\frac{1046x^{13}}{4347968625}h_7$	$\frac{1246237x^{14}}{2587041331875}h_8$
...	...	...

$$u(\vec{r},\Omega,\Omega') = u_{LJ} + u_{DD} = 4\left(\frac{1}{r^{12}} - \frac{1}{r^6}\right) + \frac{1}{2}[\vec{m}\mathbf{T}\vec{\mu}' + \vec{m}'\mathbf{T}\vec{\mu}]. \tag{A5}$$

The first term is the LJ potential. The second term describes the interaction between point dipole moments $\vec{m}$ and $\vec{m}'$, where

$$T_{\alpha\beta} = \frac{1}{r^3}(\delta_{\alpha\beta} - 3n_\alpha n_\beta) \tag{A6}$$

are the components of the dipole tensor ($\vec{n}=\vec{r}/r$). The dipole moments are given by

$$\vec{m} = \vec{\mu} - \alpha\mathbf{T}\vec{m}' \quad \text{and} \quad \vec{m}' = \vec{\mu}' - \alpha\mathbf{T}\vec{m}. \tag{A7}$$

The μ are permanent dipole moments, and α is a point polarizability. Next we express u_{DD} entirely in terms of the permanent moments and α. Using

$$\mathbf{T} = \frac{1}{r^3}\begin{pmatrix} 1 & 0 & 0 \\ 0 & 1 & 0 \\ 0 & 0 & -2 \end{pmatrix}, \tag{A8}$$

here $\vec{m}$ and $\vec{m}'$ lie on the z axis, we obtain

$$u_{DD} = \frac{1}{2}[\{(\mathbf{1} - \alpha^2\mathbf{T}^2)^{-1}(\vec{\mu} - \alpha\mathbf{T}\vec{\mu}')\}\mathbf{T}\vec{\mu}' + \{(\mathbf{1} - \alpha^2\mathbf{T}^2)^{-1}(\vec{\mu}' - \alpha\mathbf{T}\vec{\mu})\}\mathbf{T}\vec{\mu}]. \tag{A9}$$

Using $\vec{\mu}=\mu(\sin\theta\cos\phi, \sin\theta\sin\phi, \cos\theta)$ and expanding in small α yields

$$\beta u_{DD} = a(\cos\Delta\phi\sin\theta\sin\theta' - 2\cos\theta\cos\theta') - \frac{a}{r^3}[P_2(\cos\theta) + P_2(\cos\theta') + 2]\alpha + \frac{a}{r^6}(\cos\Delta\phi\sin\theta\sin\theta' - 8\cos\theta\cos\theta')\alpha^2 + \mathcal{O}(\alpha^3), \tag{A10}$$

where $a=\beta\mu^2/r^3$, $\Delta\phi=\phi-\phi'$, and P_2 is the second order Legendre polynomial. We may now carry out the integrations over ϕ and ϕ' analytically. The result may then be expanded in powers of a and the integration is carried out term by term. Notice that we assume $f(\Omega)=1$, i.e., isotropic distribution of dipole orientations. Thus the second viral coefficient $B_2(T,\mu^2,\alpha)$ becomes

$$B_2(T,\mu^2,\alpha) = B_2^{(LJ)}(T) + \frac{x^2}{3}h_1 + \frac{x^4}{25}h_2 + \cdots + \left(2xh_1 + \frac{4x^3}{5}h_2 + \cdots\right) \times \alpha + \left(\frac{21x^2}{5}h_2 + \frac{836x^4}{525}h_3 + \cdots\right)\alpha^2 + \mathcal{O}(\alpha^3). \tag{A11}$$

Here $x=\beta\mu^2$,

$$B_2^{(LJ)}(T) = -2\pi\int_0^\infty dr r^2(\exp[-\beta u_{LJ}] - 1) \tag{A12}$$

and

$$h_j = -2\pi\int_0^\infty dr r^{2-6j}\exp[-\beta u_{LJ}]. \tag{A13}$$

Additional terms in Eq. (A11) are listed in Table II.

[1] C. Holm and J.-J. Weis, Curr. Opin. Colloid Interface Sci. **10**, 133 (2005).
[2] J.-J. Weis and D. Levesque, in *Advanced Computer Simulation Approaches for Soft Matter Sciences II*, edited by C. Holm and K. Kremer, Advances in Polymer Science Vol. 185 (Springer, New York, 2005).
[3] B. Huke and M. Lücke, Rep. Prog. Phys. **67**, 1731 (2004).
[4] P. I. C. Teixeira, J. M. Tavares, and M. M. Telo da Gama, J. Phys.: Condens. Matter **12**, R411 (2000).
[5] P. G. de Gennes and P. A. Pincus, Phys. Kondens. Mater. **11**, 189 (1970).
[6] M. E. van Leeuwen and B. Smit, Phys. Rev. Lett. **71**, 3991 (1993).
[7] M. J. Stevens and G. S. Grest, Phys. Rev. E **51**, 5976 (1995).
[8] R. P. Sear, Phys. Rev. Lett. **76**, 2310 (1996).
[9] R. van Roij, Phys. Rev. Lett. **76**, 3348 (1996).
[10] J. M. Tavares, M. M. Telo da Gama, and M. A. Osipov, Phys. Rev. E **56**, R6252 (1997).
[11] J. M. Tavares, J. J. Weis, and M. M. Telo da Gama, Phys. Rev. E **59**, 4388 (1999).
[12] K. Van Workum and J. F. Douglas, Phys. Rev. E **71**, 031502 (2005).
[13] J. Dudowicz, K. F. Freed, and J. F. Douglas, Phys. Rev. Lett. **92**, 045502 (2004).
[14] R. Hentschke, J. Bartke, and F. Pesth, Phys. Rev. E **75**, 011506 (2007).
[15] P. J. Flory, *Principles of Polymer Chemisty* (Cornell University Press, Ithaca, 1953).
[16] In a previous paper [17] [Eq. (1)] the fixed dipole moment $\vec{\mu}_i$ was erroneously replaced by the full dipole moment, $\vec{m}_i$. This typing mistake did not however enter in the calculations.
[17] J. Bartke and R. Hentschke, Mol. Phys. **104**, 3057 (2006).
[18] C. G. Gray, Y. S. Sainger, C. G. Joslin, P. T. Cummings, and S. Goldmann, J. Chem. Phys. **85**, 1502 (1986).
[19] M. Neumann, Mol. Phys. **60**, 225 (1987).
[20] C. Millot, J.-C. Soetens, and M. T. C. Martins Costa, Mol. Simul. **18**, 367 (1997).
[21] D. C. Rapaport, *The Art of Molecular Dynamics Simulation* (Cambridge University Press, Cambridge, 1995).
[22] F. J. Vesely, J. Comput. Phys. **24**, 361 (1977).
[23] H. J. C. Berendsen, J. P. M. Postma, W. F. van Gunsteren, A. DiNola, and J. R. Haak, J. Chem. Phys. **81**, 3684 (1984).
[24] M. Ley-Koo and M. S. Green, Phys. Rev. A **23**, 2650 (1981).
[25] A. Pelissetto and E. Vicari, Phys. Rep. **368**, 549 (2002).
[26] D. A. Kofke, J. Chem. Phys. **98**, 4149 (1993).
[27] D. A. Kofke, Mol. Phys. **78**, 1331 (1993).
[28] P. Debye, *Polare Molekeln* (Hirzel, Leipzig, 1929).
[29] H. Zhang and M. Widom, Phys. Rev. E **49**, R3591 (1994).
[30] M. A. Pounds and P. A. Madden, J. Chem. Phys. **126**, 104506 (2007).
[31] M. E. van Leeuwen, B. Smit, and E. M. Hendriks, Mol. Phys. **78**, 271 (1993).
[32] M. E. van Leeuwen, Mol. Phys. **82**, 383 (1994).
[33] J. Stoll, J. Vrabec, and H. Hasse, Fluid Phase Equilib. **209**, 29 (2003).
[34] Z. Lu, W. Ouyang, Z. Sun, Z. Li, and L. An, Chin. Sci. Bull. **50**, 1595 (2005).
[35] B. Groh and S. Dietrich, Phys. Rev. E **50**, 3814 (1994).
[36] B. Groh and S. Dietrich, Phys. Rev. Lett. **72**, 2422 (1994).
[37] G. T. Gao and X. C. Zeng, Phys. Rev. E **61**, R2188 (2000).
[38] L. Onsager, Ann. N.Y. Acad. Sci. **51**, 627 (1949).
[39] A. Yu. Grosberg and A. R. Khokhlov, *Soviet Scientific Reviews, Physics Reviews* (Harwood Academic, London), 8, 5–156 (1987).
[40] A. N. Semenov and A. R. Khokhlov, Sov. Phys. Usp. **31**, 988 (1989).
[41] T. Odijk, Curr. Opin. Colloid Interface Sci. **1**, 337 (1996).
[42] J. T. Kindt and W. M. Gelbart, J. Chem. Phys. **114**, 1432 (2001).
[43] R. Hentschke, P. Lenz, and B. Fodi, in *Supramolecular Polymers*, edited by A. Cifferri (Taylor & Francis, Boca Raton, 2005).
[44] H. Yamakawa and W. H. Stockmayer, J. Chem. Phys. **57**, 2843 (1972).
[45] T. Tlusty and S. A. Safran, Science **290**, 1328 (2000).
[46] R. Zwanzig, J. Chem. Phys. **39**, 1714 (1963).
[47] W. Pauli, *Statistical Mechanics* (Dover, Mineola, 1973).